Proceedings of the Institute of Acoustics

HARMONIC DISTORTION IN LOUDSPEAKERS DUE TO MAGNETIC HYSTERESIS AND EDDY CURRENTS

Nick Merricks

Loudspeaker Technology Ltd., Gypsy Lane, Aston Down, Stroud, Gloucestershire.

1 INTRODUCTION

One of the primary sources of non-linear behaviour in certain types of loudspeaker comes from the interaction of the magnetic field produced by the voice coil, induced eddy currents and the hysteresis of the material used to form the magnetic circuit of the drive system. Much work has been done in this field with the aims of modelling the effects and reducing the non-linear distortion that may result from them [1]–[6]. Experiments performed on the ATC SB75-150 loudspeaker drive unit (L.D.U.) have shown that by replacing the steel surrounding the magnetic gap with a material of low conductivity and high permeability, the third harmonic distortion in the acoustic output is reduced by a significant factor (10-15dB) between 100Hz and 3kHz. In a series of experiments to investigate the magnetic distortion, mechanical effects have been eliminated by removing the permanent magnetic field[1], mounting the coil in the quiescent position and observing the harmonic components of the current passing through it. An attempt to explain the harmonic distortion by means of an analytical model of the electromagnetic processes occurring in the magnetic drive system of the loudspeaker is presented. Predictions of the following have been sought:

- Variation of coil impedance with frequency, taking into account the effect of eddy currents.
- Electric and magnetic field strengths as functions of position within regions surrounding the voice coil.

These results have been used to form conclusions concerning the harmonic frequency components of the e.m.f. induced in the voice coil due to the hysteresis of the surrounding material and induced eddy currents.
The analysis is based on the observation that the voice coil used in the ATC SB75-150 is relatively short in comparison with the magnetic gap and so the system is modelled as a coil surrounded by an arbitrary number of infinitely long, coaxial layers of material. The linear field equations for this geometry have been derived and used to calculate the magnetisation in the surrounding regions at the fundamental frequency, as well as the complex impedance of the coil. Harmonic excitations due to the non-linear material characteristics are introduced by a perturbation method, finally resulting in

[1] This was achieved by omitting the magnet energising procedure during production.

expressions for the harmonic components of the e.m.f. induced in the coil. The equations governing the electromagnetic behaviour have been computer coded in order to calculate numerical results. These data are compared with experimental measurements for frequencies up to 5kHz. Simple configurations have been examined initially to provide experimental support for the more complex models.

2 SYSTEM CONFIGURATION

The L.D.U. under investigation, the ATC SB75-150, is of the 'short coil, long magnetic gap' type comprising a 75mm diameter voice coil with 55 turns of copper wire, and 8mm in length, operating in a magnetic gap of 20mm length. The magnetic circuit comprises an annular ceramic magnet sandwiched between EN3A grade mild steel which is electroplated with a zinc treatment of approximately 5 microns thickness.
Reference has been made earlier in the text to a material of high permeability and low conductivity, which has been added to the standard magnetic circuit of the L.D.U., (Figure 2.1). This material is an iron powder polymer composite and is formed from powdered iron particles, each of which is coated with an insulating layer of oxide. In manufacture, the powder is formed into a solid by bonding with a phenolic resin under high pressure. For the purpose of distortion reduction in the L.D.U., the iron powder is formed into rings and fitted into place around the voice coil. This configuration is known as 'tipped'.

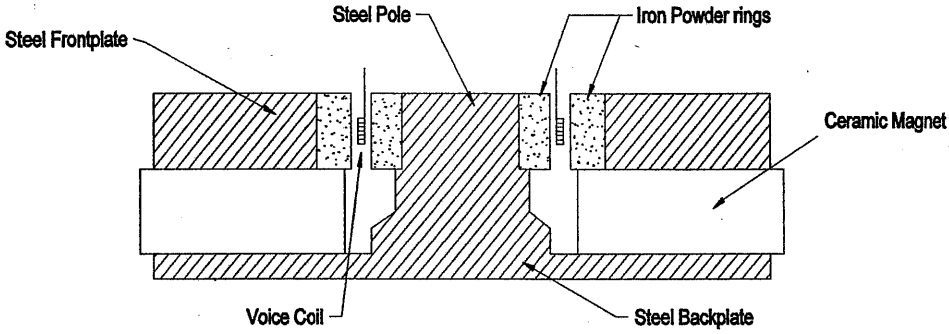

Figure 2.1 Magnetic circuit (drive system) of the tipped ATC SB75-150 L.D.U..

3 FIELD THEORY

An analytical model suitable for a short coil, long gap loudspeaker has been described by Dodd, Cheng and Deeds [7] in which the coil is surrounded by an arbitrary number of infinitely long coaxial layers, each with their own independent permeability μ and conductivity σ. The linear analysis provides expressions for the impedance of the coil Z and the vector potential $\boldsymbol{A}$ in the coaxial layers due to a harmonic current I in the voice coil at an arbitrary frequency ω. Varying the number of layers allows modelling of the tipped and untipped systems. The expressions given by [7] have been extended by Harfield and Bowler [8] to give the linear equations for electric field E and the magnetic field H as functions of layer and position within the layers, and also as functions of frequency.

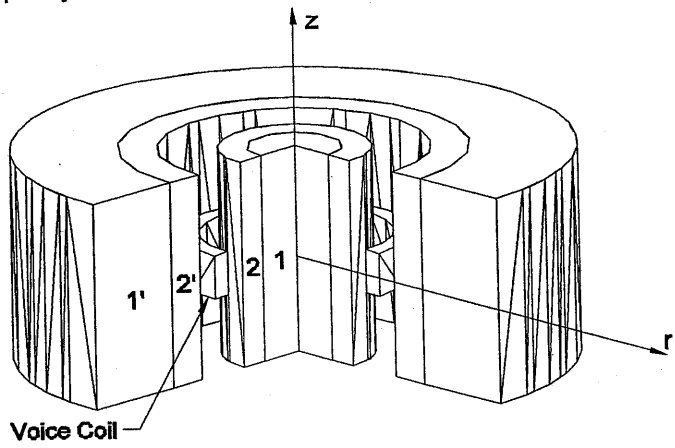

Figure 3.1 Geometry of Dodd, Cheng and Deeds analysis.

Note that in the cylindrical system, the electric field has only azimuthal components and the magnetic field has only radial and axial components. The numbers within the layer boundaries in Figure 3.1 identify the layer, with primed numbers indicating regions outside the coil, and unprimed numbers identifying regions within. Region 1' is assumed to extend outwards to infinity. The coil has N turns and is centred in the z-direction at z=0.

Non-linear distortion is explained in terms of a cubic equation relating the magnetic field and the magnetic flux density [8]. The linear analysis and experimental results are used to provide an explanation of the mechanisms involved in the reduction of distortion by the tipping procedure.

3.1 Linear Analysis

The vector potential equation for regions inside the coil as given in [8] is,

$$A^{(n)}(r,z)=\frac{NI\mu_0}{\pi}\int_0^{\infty}\left\{\frac{\left[U_{12}I(R_2,R_1)+U_{22}K(R_2,R_1)\right]}{\alpha\alpha_0^2\left(U_{22}V_{11}-U_{12}V_{21}\right)}\left[V_{11}(n)I_1(\alpha_n r)+V_{21}(n)K_1(\alpha_n r)\right]\times\right.$$
$$\left.\left[\sin\alpha(z-l_1)-\sin\alpha(z-l_2)\right]\right\}d\alpha \qquad (1)$$

and for regions outside the coil,

$$A^{(n')}(r,z)=\frac{NI\mu_0}{\pi}\int_0^{\infty}\left\{\frac{\left[V_{11}I(R_2,R_1)+V_{21}K(R_2,R_1)\right]}{\alpha\alpha_0^2\left(U_{22}V_{11}-U_{12}V_{21}\right)}\left[U_{12}(n')I_1(\alpha_{n'}r)+U_{22}(n')K_1(\alpha_{n'}r)\right]\times\right.$$
$$\left.\left[\sin\alpha(z-l_1)-\sin\alpha(z-l_2)\right]\right\}d\alpha \qquad (2)$$

where,

l_1, l_2, co-ordinates of the coil base and top respectively

R_1, R_2, inner and outer coil radii respectively

$\alpha_n=\left(\alpha^2-i\omega\mu_0\mu_{rn}\sigma_n\right)^{1/2}$ with

μ_{rn}, relative permeability of region n

σ_n, conductivity of region n

U_{ij}, V_{ij}, matrix elements defined in Appendix A

$I_j(x)$, $K_j(x)$, modified Bessel functions of order j

$I(R_2,R_1)$, $K(R_2,R_1)$, functions related to finite coil size and defined by

$$I\left(R_2,R_1\right)=\alpha_0^2\int_{R_1}^{R_2}rI_1\left(\alpha_0 r\right)dr \qquad (3)$$

$$K\left(R_2,R_1\right)=\alpha_0^2\int_{R_1}^{R_2}rK_1\left(\alpha_0 r\right)dr \qquad (4)$$

Making the assumption that all the materials comprising the system are linear, isotropic and homogeneous allows the electric and magnetic fields to be derived from the relations,

$$E_\phi=i\omega A_\phi \qquad (5)$$

and,

$$H=\frac{1}{\mu_0\mu_{rn}}\nabla\times\hat{\phi}A_\phi \qquad (6)$$

together with equations (1) and (2). The general equation for the impedance of the coil is,

$$Z = -2i\omega N^2 \mu_0 \int_0^\infty \left(\frac{\pi}{\alpha^3 \alpha_0^3} \left\{ \alpha_0 (l_2 - l_1) + \exp\left[-\alpha_0 (l_2 - l_1) \right] - 1 \right\} J^2(R_2, R_1) \right.$$
$$\left. + \frac{2\left[1 - \cos\alpha(l_2 - l_1)\right]}{\alpha^2 \alpha_0^4} \left[\frac{U_{12}V_{11}I^2(R_2,R_1) + U_{22}V_{21}K^2(R_2,R_1) + 2U_{12}V_{21}I(R_2,R_1)K(R_2,R_1)}{U_{22}V_{11} - U_{12}V_{21}} \right] \right) d\alpha \quad (7)$$

where $J(R_2,R_1)$ is defined in terms of the modified Bessel function J_1 as,

$$J(R_2, R_1) = \alpha_0^2 \int_{R_1}^{R_2} r J_1(\alpha_0 r) dr \quad (8)$$

These equations are adapted to the particular configuration to be modelled by altering the number of layers inside and outside of the coil, the dimensions of the layers and their material properties. Explicit forms suitable for situations described here are given in [8].

3.2 Non-Linear Analysis

The non-linear relationship between the magnetic field ***H*** and the magnetic flux density *B* in the layers surrounding the coil is given by,

$$B(r,t) = \mu H(r) e^{i\omega t} + \beta^{(2)} \left[H(r) \right]^2 e^{i2\omega t} + \beta^{(3)} \left[H(r) \right]^3 e^{i3\omega t} \quad (9)$$

where $\beta^{(n)}$ are the small parameters used to define the non-linear behaviour of the magnetic materials. In vector form,

$$B(r,t) = \mu H(r) e^{i\omega t} + M^{(2)}(r) e^{i2\omega t} + M^{(3)}(r) e^{i3\omega t} \quad (10)$$

where the magnetisation

$$M^{(j)} = \hat{r} M_r^j + \hat{z} M_z^j = \hat{r} \beta^{(j)} H_r^j + \hat{z} \beta^{(j)} H_z^j \quad (11)$$

contains the radial and axial components of the magnetic field for the j^{th} harmonic. The magnetisation may be used to calculate the e.m.f. V^j induced in the coil at the harmonic frequencies. This calculation is performed by making the approximation that ***M*** is piecewise constant within a ring element of rectangular cross-section and summing the piecewise contributions over all the discrete elements within each layer,

indexed by ρ and ζ. The e.m.f. induced in the coil may be expressed in terms of the magnetisation and Green's functions G^{ϕ} as,

$$V^j = 2\pi N\left[\sum_{\rho=1}^{n_r}\sum_{\zeta=1}^{n_z} M_r^{j,\rho,\zeta}\int_{z_\zeta}^{z_\zeta+\delta_z}\int_{r_\rho}^{r_\rho+\delta_\rho} G^{\phi}(r',z')r'dr'dz' + \sum_{\rho=1}^{n_r}\sum_{\zeta=1}^{n_z} M_z^{j,\rho,\zeta}\int_{z_\zeta}^{z_\zeta+\delta_z}\int_{r_\rho}^{r_\rho+\delta_\rho} G^{\phi}(r',z')r'dr'dz'\right] \quad \textbf{(12)}$$

where $z_\zeta = \frac{1}{2}\left(l_1 - l_2 - n_z\delta_z\right) + \zeta\delta_z$ and $r_\rho = r_i + \rho\delta_\rho$, the integrations being performed over the discrete cell dimensions δ_r and δ_z. See Appendix B for explicit forms of equation (12).

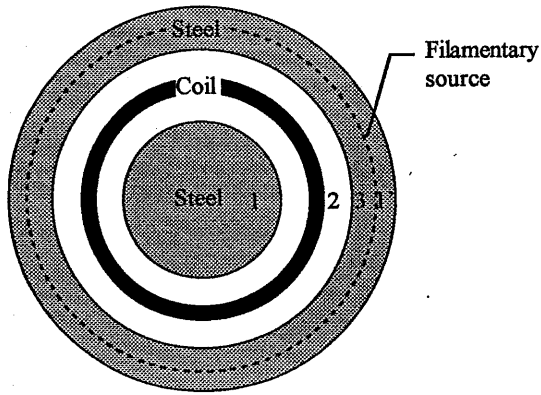

Figure 3.2 Plan view of the untipped configuration including a filamentary source of constant magnetisation. The layers are numbered relative to the filamentary source (compare with Figure 3.1).

4 IMPEDANCE MODEL

4.1 Impedance Simulations

The explicit versions of the equations in section 3 relating to each configuration to be modelled have been coded into a FORTRAN computer program, allowing each of the independent parameters to be varied according to the situation under investigation. The simplest configuration modelled is that of a cylindrical steel pole surrounded by a coil. The complex impedance variation with frequency of the coil in this situation was calculated and compared with the experimental result. For a skin depth which is small in comparison with the radius of the coil, the impedance characteristic for a particular geometry depends only on the value of μ/σ and so this value was altered in order to match the experimental and calculated data, giving the ratio for the steel being used. This ratio was then used for the steel in more complicated configurations. The ratio of permeability to conductivity found in this way was similar to the value given by Kaye and Laby [9] for carbon steel. The same procedure was performed on a cylinder of iron powder, although the permeability and conductivity have to be fitted independently because the skin depth is large due to the low conductivity. This provided the parameters needed to perform further linear simulations of the magnetic circuit.

4.2 Impedance Measurements

The impedance measurements were carried out using an impedance analyser connected to an SB75-150 voice coil. This was mounted concentrically over a 250mm long cylinder of EN3A grade steel with the same diameter as the pole of the SB75-150. A pole length of 250mm was used in order to ensure that the end effects were negligible. The analyser was estimated to be accurate to ±3%. Capacitive effects of the voice coil windings were tested on a bridge and found to be negligible at 1kHz.

Figure 4.1 shows the good agreement between theoretical and experimental results when μ_r=160 and σ=5.5 x 10^6 S·m^{-1}. Note that the DC resistance of the coil (about 5.4Ω) has been subtracted from the real part of the measured data to leave just the in-phase component of impedance due to the back e.m.f. caused by the eddy currents induced in the steel pole. The calculated real part is in error by about 8% of the experimental value at the upper frequency limit of 5kHz and the imaginary part is in error by less than the 3% tolerance.

The result of the iron powder experiment is shown in Figure 4.2. Again, a pole of material 250mm in length was used to approximate the effect of an infinite pole. The best fit to the impedance data was found for μ_r=25 and σ=5.0 S·m^{-1}, for which the calculated impedance is well within ±3% of the measured data. It is evident from this graph that the suppression of the eddy currents has resulted in a large reduction of the real part of the impedance compared to the steel pole case, and the imaginary part has increased roughly threefold at 5kHz. This can be explained by considering the inductive and resistive effects separately. In an inductor, a ferromagnetic core may be

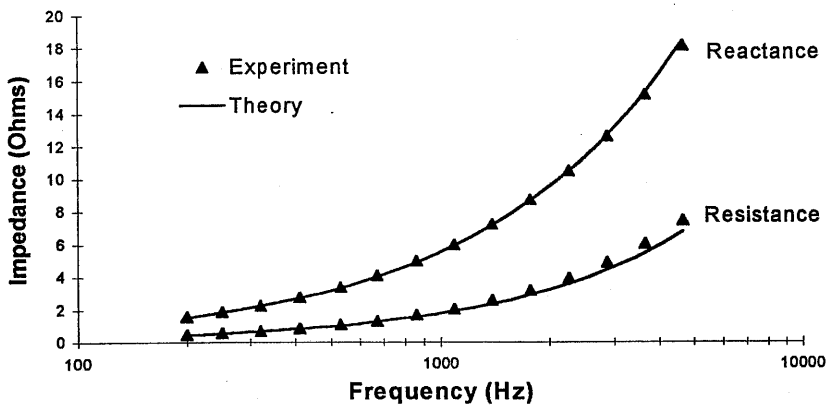

Figure 4.1 Comparison of calculated and measured impedance of SB75-150 voice coil on a steel pole.

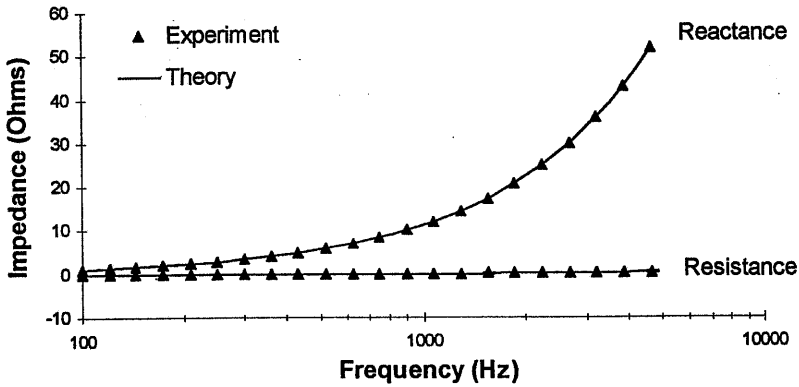

Figure 4.2 Comparison of calculated and measured impedance of SB75-150 voice coil on an iron powder pole.

used to increase the flux linkage within the windings, and thus the value of self-inductance. However, any eddy currents circulating within the core will act as a 'shield' against the flux [10], lowering the self-inductance in accordance with Lenz's law, and for steel it is this effect which dominates. We observe this behaviour from the graphs. The real part of the impedance is subject only to the in-phase component of the back e.m.f. (due to the eddy currents) which, by Lenz's law, will be opposing the flux producing it. In the presence of eddy currents (a steel core) this e.m.f. will act to increase the resistance. Without the eddy currents (the case of an iron powder core) there will be no such effect. The effect on the resistance can also be explained in terms of an energy loss. The I^2R dissipation in the steel will greatly exceed that in the iron powder because of the presence of eddy currents, and this is reflected in the real part of the driving point impedance of the voice coil.

Knowledge of the permeability and conductivity of the materials from infinite pole measurements allows predictions to be made of the impedance of the voice coil within the magnetic circuit of the drive unit. The first of these impedance characterisations is of the voice coil in the untipped configuration and corresponds to three layers inside and outside the coil, the air gap, the zinc coating[2] and the steel pole. Impedance measurements were prepared by gluing the coil as centrally as possible in the gap, both concentrically and along its length, and the results are shown in Figure 4.3. A small deviation from the measurement of 5% is observed in the reactive component at high frequencies, the resistance remaining within tolerance. This may be attributable to the coil not being quite concentric with the gap. Unfortunately the limited number of samples available did not allow the experimental error to be ascertained, but an idea of the sensitivity of the model to misalignment may be found by altering the coil radius and recalculating the results. Simulation of the untipped system with a diameter 1mm less than the actual diameter changes the impedance by up to 9%. Although the model can only make predictions for coaxial configurations, if changing the distance from the coil to the core by 0.5mm causes the prediction to vary by such an amount, it is not unreasonable to assume that any errors in the concentricity of the apparatus will lead to a similar percentage error.

Finally the tipped system was simulated and the results found to agree with the measured data to within the experimental tolerance. Comparing the result with that from the iron powder pole experiment in Figure 4.2 suggests that the tipping material is the dominating factor in the impedance characteristic, the steel making an insignificant contribution.

[2] The zinc coating was assumed to have a conductivity of 16.9×10^6 S·m^{-1} [9] and a relative permeability of 1.0.

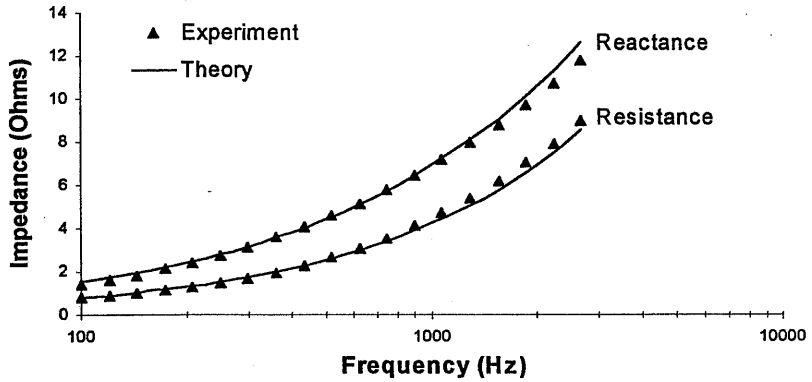

Figure 4.3 Result of the untipped configuration simulation and the corresponding measured data.

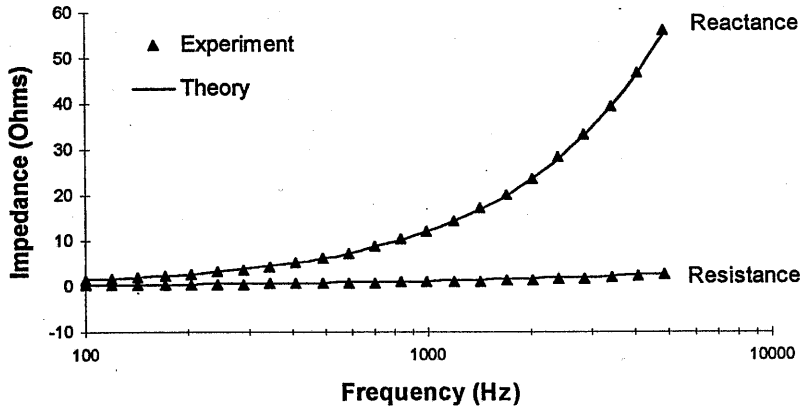

Figure 4.4 Measured and calculated impedance of the coil in the tipped configuration.

5 ELECTROMAGNETIC FIELD MODELS

5.1 Electric Field

The Minowski formulation of the Maxwell equation

$$\nabla \times \boldsymbol{E} + \frac{\partial \boldsymbol{B}}{\partial t} = 0 \qquad (13)$$

is written

$$\nabla \times \boldsymbol{E} + j\omega\mu\boldsymbol{H} = 0 \qquad (14)$$

from which it can be seen that the contour diagram of the electric field within the regions adjacent to the coil will provide the 'picture' of the magnetic field strength in those regions for a sinusoidally varying field.

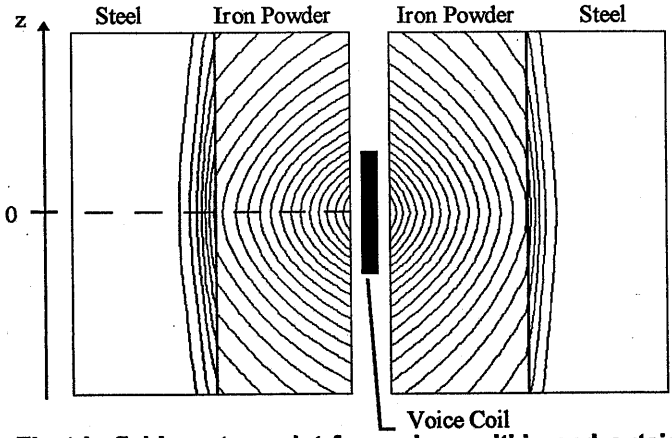

Figure 5.1 Electric field contour plot for regions within and outside the voice coil in the tipped configuration at 500Hz.

This prediction was made by evaluating the electric field at 500Hz using equation (5) for discrete positions within the layers, limited in the radial direction to 14mm inside the coil, 14mm outside and 10mm either side of the coil in the axial direction. From the electric field diagram (Figure 5.1) it may be seen that the magnetic field remains fairly constant within the iron powder regions, whilst dropping off rapidly in the steel in accordance with the skin effect.

5.2 Magnetic Field

Using equation (6) the radial and axial components of the magnetic field may be predicted for discrete positions within the layers. From Figure 5.1 it may be noticed that the magnetic field is dominated by the axial component at z=0, and this is confirmed by the model predictions. Only the axial component will be presented here. Firstly, the magnetic field for the simple configuration of a coil surrounding an infinite pole of radius 37.2mm will be presented. The field magnitude variation over a suitable range of r is predicted for the z=0 plane at 500Hz and the result given in Figure 5.2.

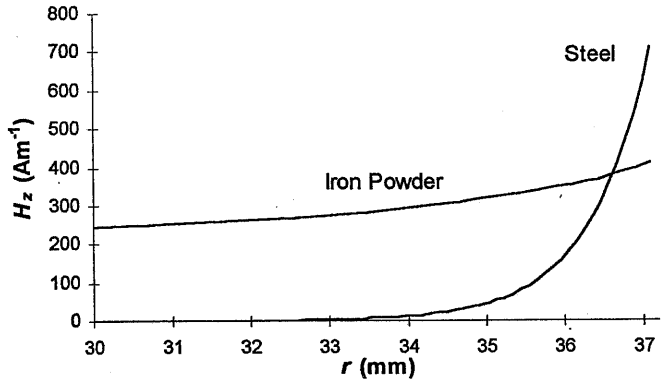

Figure 5.2 Prediction of axial component of magnetic field variation with r for z=0 within infinite cylinders of iron powder and steel at 500 Hz.

It is clear from the graph that the magnetic field is almost halved when the steel is replaced by iron powder. This may be attributed to the low conductivity of the iron powder which, by suppressing the eddy currents within, also suppresses the magnetic field associated with them. Figure 5.3 shows the magnetic field variation along the radial direction at z=0 for regions inside the coil in the tipped and untipped configurations, again at 500Hz. This is clarified by the dashed line in Figure 5.1. It is clear from the figure that the maximum value of the magnetic field at the surface of the layer closest to the coil is largely unaffected by the iron powder tipping. Although the eddy currents, and their associated magnetic field, have been suppressed, the field level in the tipped metalwork is maintained at a level similar to that within the untipped metalwork. The field in the tipped regions appears to be maintained by the steel pole and frontplate behind them.

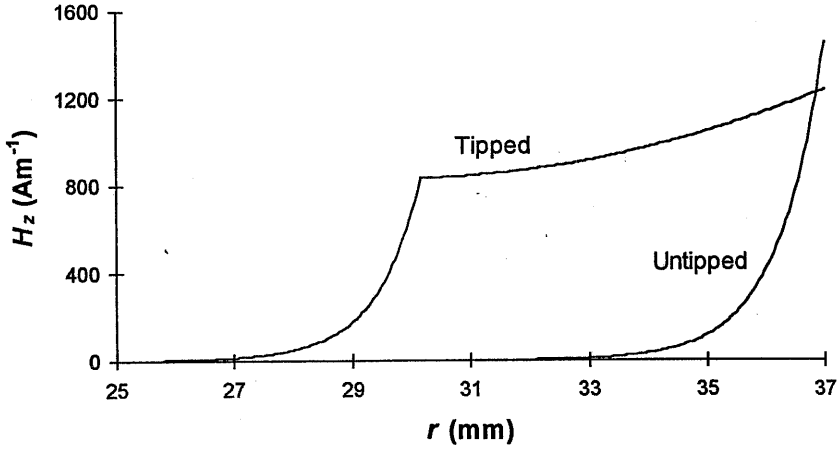

Figure 5.3 Magnetic field variation with *r* at *z*=0 for tipped and untipped systems at 500 Hz.

6 NON-LINEAR FACTORS

Linear analysis has provided much information about the electromagnetic interactions occurring within the loudspeaker. This knowledge is now collated into an argument for the explanation of the effect described in the introduction - the reduction of the non-linear distortion by the tipping process.

Figure 6.1 shows the third harmonic distortion of the SB75-150 L.D.U. which was measured with a Fast Fourier analyser. A constant current of 1 Amp was passed through the voice coil and the voltage developed across a 0.1Ω series resistor measured at the harmonic frequency. The results are scaled in dB units, relative to the fundamental current.

Although the non-linear analysis in section 3.2 may be implemented in the same way as the linear model, we will be content here with a qualitative description of the non-linear behaviour.

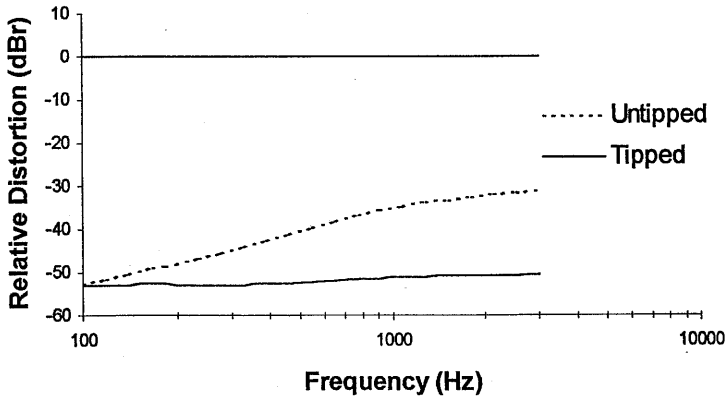

Figure 6.1 Third harmonic distortion of SB75-150 L.D.U. drive systems in tipped and untipped configurations. Graph shows third harmonic component of the currents passing through the voice coils with reference to the constant 1 Amp fundamental current.

There are two obvious possible explanations for the difference in non-linearity between the two systems,

- The iron powder is intrinsically more linear - that is the β coefficients in equation (9) are smaller for iron powder than for steel.
- The magnetic field in the iron powder is lower than in the steel, bringing the magnetisation down into a more linear region of the hysteresis curve.

Unfortunately, there is no evidence to suggest that the first point above is the case, although iron powder is not expected to be significantly more linear than steel. A rigorous analysis needs to be performed to gain the β coefficients for each material. The magnetic field level within the layers would influence the distortion levels via the hysteresis curve of the materials. Section 5.2 has shown that the magnetic field within the regions adjacent to the coil is not greatly affected by the presence of the tipping material, it providing a reduction of around 12% at the surface adjacent to the coil. This reduction in the field would not be expected to lead to such a dramatic drop in the distortion levels.

Returning to the impedance analysis and noting that the magnitude of Z is generally higher for tipped configurations than for untipped reveals another possibility for an explanation of the effect. Within their operational bandwidth, the acoustical output of dynamic loudspeakers is generally constant with the force on the voice coil, given by,

$$F = BIl \tag{15}$$

where B is the constant magnetic induction in Teslas provided by the permanent magnet, I is the current passing through the voice coil and l is the length of wire comprising the voice coil. Putting the equation in terms of the voltage V across the coil and the coil impedance Z gives,

$$F = \frac{BVl}{Z} \tag{16}$$

For both tipped and untipped configurations the permanent field B and the length of wire l are nominally the same. Compare the two systems when driven by a constant current of 1 Amp. At the fundamental frequency, the impedance of the tipped configuration is roughly three times that of the untipped system, and the voltage across the coil will be equal to the impedance for unity current drive. However, reference to equation (12) shows that the harmonic components induced in the coil are independent of this linear impedance and they will be affected only by the β coefficients for each material and the magnetic field within that material. Rather than the tipping process reducing the distortion components produced by the hysteresis, it is raising the fundamental signal, leaving the distortion at a lower relative level. The impedance of the tipped system is roughly three times that of the untipped system over much of the frequency range and one would therefore expect a threefold reduction of the relative distortion levels. This is equivalent to $20\log(3) \approx 10dB$ which is the order of improvement observed. It should be noted that the magnetic field in the tipped drive system is slightly lower than that in the untipped system, and this will have some positive effect on the distortion, albeit marginal in comparison to the improvement provided by the impedance rise.

The rise in impedance is not without its own disadvantages, such as the reduction in bandwidth of the acoustic output. These effects will need to be considered at the design stage.

7 CONCLUSION

A linear theory for the prediction of the electromagnetic properties of long gap, short coil dynamic loudspeakers has been presented. Investigations have been made on blocked voice coil systems with the permanent magnetic field removed. Impedance predictions have been shown to match experimental observations to a good degree of accuracy and electric and magnetic fields calculated for regions within the magnetic circuit of the loudspeaker. The knowledge gained from linear analysis of the ATC SB75-150 L.D.U. has been used to explain the non-linear processes occurring within

the loudspeaker, with reference to the reduction in distortion levels when the steel regions surrounding the coil are replaced with a material of high permeability and low conductivity, known as iron powder. It has been suggested that the reduction is primarily due to the rise in impedance associated with the addition of iron powder rings to the magnetic circuit.

Further work is required to ascertain the β coefficients for the steel and iron powder materials in order that the intrinsic non-linearity of these materials may be compared. It is hoped that future investigations will address this, and other questions, including the contribution made by the permanent magnetic field.

8 REFERENCES

[1] Olson, H. F., *Acoustical Engineering*, Professional Audio Journals Inc., Philadelphia, Pennsylvania, 1991.

[2] McLachlan, N. W., *Ordinary Non-Linear Differential Equations in Engineering and Physical Sciences*, Oxford University Press, London, 1950.

[3] Cunningham, W. J., Non-Linear Distortion in Dynamic Loudspeakers due to Magnetic Effects, *Journal of the Acoustical Society of America*, 21(3), 1949.

[4] Tsuchiya, H., Okada, N. and Saaki, T., Reducing Harmonic Distortion in Loudspeakers, presented at *the 63rd Convention of the Audio Engineering Society*, May 1979, preprint 1488.

[5] Vanderkooy, J., A Model of Loudspeaker Driving Impedance Incorporating Eddy Currents in the Pole Structure, *Journal of the Audio Engineering Society*, Vol. 37, N 3, 1989, March, pp. 119-128.

[6] Aldoshina, I., Voishvillo, A. and Mazin, V., Loudspeaker Motor Non-Linear Modelling Based on Calculated Magnetic Field Inside the Gap, presented at the 97th Convention of the Audio Engineering Society, *J. Audio Eng. Soc.*, (Abstracts) vol. 42, N 12, 1994, December, pp 1061-1062, preprint 3895.

[7] Dodd, C. V., Cheng, C. C. and Deeds, W. E., Induction Coils Coaxial with an Arbitrary Number of Cylindrical Conductors, *J. Appl. Phys.*, 45(2), 638-647, 1974.

[8] Harfield, N., Bowler, J. R., *Harmonic Distortion in Loudspeakers due to Magnetic Hysteresis*, project report carried out by EM Imaging Systems under a contract with ATC Loudspeaker Technology Limited, August 1996.

[9] Kaye, G. W. C., Laby, T. H., *Tables of Physical and Chemical Constants*, 14th Edition, Longman, London, 1973.

[10] Scott, K. L., Variation of the Inductance of Coils due to the Magnetic Shielding Effects of Eddy Currents in the Cores, *Proceedings of the Institute of Radio Engineers*, 18(10), pp1750-1764, October 1930.

APPENDIX A

$\tilde{V}(n)$ and $\tilde{U}(n')$ are matrices of the form,

$$\tilde{V}(n) = \begin{bmatrix} V_{11}(n) & V_{12}(n) \\ V_{21}(n) & V_{22}(n) \end{bmatrix}$$

$$\tilde{U}(n') = \begin{bmatrix} U_{11}(n') & U_{12}(n') \\ U_{21}(n') & U_{22}(n') \end{bmatrix}$$

For an integer value of n,

$$\tilde{V}(n) = \tilde{T}_{n,n-1}\tilde{T}_{n-1,n-2}\ldots\tilde{T}_{3,2}\tilde{T}_{2,1}$$

$$\tilde{U}(n') = \tilde{T}_{n',n'-1}\tilde{T}_{n'-1,n'-2}\ldots\tilde{T}_{3',2'}\tilde{T}_{2',1'}$$

where the $\tilde{T}$ are 2 x 2 transformation matrices:

$$\tilde{T}_{n+1,n} = \begin{bmatrix} T_{11}(n+1,n) & T_{12}(n+1,n) \\ T_{21}(n+1,n) & T_{22}(n+1,n) \end{bmatrix}$$

whose elements are

$$T_{11}(n+1,n) = \left[K_0(\alpha_{n+1}r_n)I_1(\alpha_n r_n) + (b_n / b_{n+1})I_0(\alpha_n r_n)K_1(\alpha_{n+1}r_n)\right]\alpha_{n+1}r_n$$

$$T_{12}(n+1,n) = \left[K_0(\alpha_{n+1}r_n)K_1(\alpha_n r_n) - (b_n / b_{n+1})K_0(\alpha_n r_n)K_1(\alpha_{n+1}r_n)\right]\alpha_{n+1}r_n$$

$$T_{21}(n+1,n) = \left[I_0(\alpha_{n+1}r_n)I_1(\alpha_n r_n) - (b_n / b_{n+1})I_0(\alpha_n r_n)I_1(\alpha_{n+1}r_n)\right]\alpha_{n+1}r_n$$

$$T_{22}(n+1,n) = \left[I_0(\alpha_{n+1}r_n)K_1(\alpha_n r_n) + (b_n / b_{n+1})K_0(\alpha_n r_n)I_1(\alpha_{n+1}r_n)\right]\alpha_{n+1}r_n$$

and $b_n = \alpha_n / \mu_m$

r_n is the radius of the interface (nearest the coil) of layer *n*.

APPENDIX B

The explicit form of equation (12) for regions outside the coil is,

$$V_n^j = 4N\left\{\sum_{\rho=1}^{n_r}\sum_{\zeta=1}^{n_z} M_r^{j,\rho,\zeta}\int_0^\infty \frac{\left[V_{11}(n)I(\alpha_n,R_2,R_1)+V_{21}(n)K(\alpha_n,R_2,R_1)\right]}{\alpha\alpha_n^2\alpha_s^2\left[U_{22}V_{11}-U_{12}V_{21}\right]}\times\right.$$
$$\left[U_{12}I'(\alpha_s,\delta_r,r_i)+U_{22}K'(\alpha_s,\delta_r,r_i)\right]\times$$
$$\sin\frac{\alpha}{2}(l_1-l_2)\left[\cos\alpha\delta_z\left(\frac{n_z}{2}-\zeta\right)-\cos\alpha\delta_z\left(\frac{n_z}{2}-\zeta+1\right)\right]d\alpha$$
$$+\sum_{\rho=1}^{n_r}\sum_{\zeta=1}^{n_z} M_z^{j,\rho,\zeta}\int_0^\infty \frac{\left[V_{11}(n)I(\alpha_n,R_2,R_1)+V_{21}(n)K(\alpha_n,R_2,R_1)\right]}{\alpha^2\alpha_n^2\left[U_{22}V_{11}-U_{12}V_{21}\right]}\times$$
$$\left[U_{12}I''(\alpha_s,\delta_r,r_i)+U_{22}K''(\alpha_s,\delta_r,r_i)\right]\times$$
$$\left.\sin\frac{\alpha}{2}(l_1-l_2)\left[\sin\alpha\delta_z\left(\frac{n_z}{2}-\zeta\right)-\sin\alpha\delta_z\left(\frac{n_z}{2}-\zeta+1\right)\right]d\alpha\right\}$$

and for regions inside the coil,

$$V_{n'}^j = 4N\left\{\sum_{\rho=1}^{n_r}\sum_{\zeta=1}^{n_z} M_r^{j,\rho,\zeta}\int_0^\infty \frac{\left[U_2(n')I(\alpha_{n'},R_2,R_1)+U_{22}(n')K(\alpha_{n'},R_2,R_1)\right]}{\alpha\alpha_{n'}^2\alpha_s^2\left[U_{22}V_{11}-U_{12}V_{21}\right]}\times\right.$$
$$\left[V_{11}I'(\alpha_s,\delta_r',r_i)+V_{21}K'(\alpha_s,\delta_r',r_i)\right]\times$$
$$\sin\frac{\alpha}{2}(l_1-l_2)\left[\cos\alpha\delta_z\left(\frac{n_z}{2}-\zeta\right)-\cos\alpha\delta_z\left(\frac{n_z}{2}-\zeta+1\right)\right]d\alpha$$
$$+\sum_{\rho=1}^{n_r}\sum_{\zeta=1}^{n_z} M_z^{j,\rho,\zeta}\int_0^\infty \frac{\left[U_{12}(n')I(\alpha_{n'},R_2,R_1)+U_{22}(n')K(\alpha_{n'},R_2,R_1)\right]}{\alpha^2\alpha_{n'}^2\left[U_{22}V_{11}-U_{12}V_{21}\right]}\times$$
$$\left[V_{11}I''(\alpha_s,\delta_r',r_i)+V_{21}K''(\alpha_s,\delta_r',r_i)\right]\times$$
$$\left.\sin\frac{\alpha}{2}(l_1-l_2)\left[\sin\alpha\delta_z\left(\frac{n_z}{2}-\zeta\right)-\sin\alpha\delta_z\left(\frac{n_z}{2}-\zeta+1\right)\right]d\alpha\right\}$$

$$I'(\alpha_s,\delta_r,r_i) = -(r_i+\rho\delta_r)\{2I_1[\alpha_s(r_i+\rho\delta_r)] - \alpha_s(r_i+\rho\delta_r)I_0[\alpha_s(r_i+\rho\delta_r)]\}$$

where

$$+[r_i+(\rho-1)\delta_r]\{2I_1\{\alpha_s[r_i+(\rho-1)\delta_r]\} - \alpha_s[r_i+(\rho-1)\delta_r]I_0\{\alpha_s[r_i+(\rho-1)\delta_r]\}\}$$

$$K'(\alpha_s,\delta_r,r_i) = -(r_i+\rho\delta_r)\{2K_1[\alpha_s(r_i+\rho\delta_r)] + \alpha_s(r_i+\rho\delta_r)K_0[\alpha_s(r_i+\rho\delta_r)]\}$$

$$+[r_i+(\rho-1)\delta_r]\{2K_1\{\alpha_s[r_i+(\rho-1)\delta_r]\} + \alpha_s[r_i+(\rho-1)\delta_r]K_0\{\alpha_s[r_i+(\rho-1)\delta_r]\}\}$$

$$I''(\alpha_s,\delta_r,r_i) = (r_i+\rho\delta_r)^2 I_1[\alpha_s(r_i+\rho\delta_r)] - [r_i+(\rho-1)\delta_r]^2 I_1\{\alpha_s[r_i+(\rho-1)\delta_r]\}$$

$$K''(\alpha_s,\delta_r,r_i) = (r_i+\rho\delta_r)^2 K_1[\alpha_s(r_i+\rho\delta_r)] - [r_i+(\rho-1)\delta_r]^2 K_1\{\alpha_s[r_i+(\rho-1)\delta_r]\}$$

For regions within the coil, the cell length in the radial direction is denoted by δ_r' and for regions outside the coil, δ_r. The position of the surface of the region of interest closer to the coil is denoted by r_i, and by convention δ_r' is negative and δ_r is positive.